

# EFFECTS OF HYDROGEN ON THE FRACTURE TOUGHNESS OF CrMo AND CrMoV STEELS QUENCHED AND TEMPERED AT DIFFERENT TEMPERATURES

L.B. Peral \*, A. Zafra<sup>1\*</sup>, J. Belzunce\* and C. Rodríguez\*

<sup>1</sup>Corresponding author: A. Zafra (+34 985182023) alfredyzafr@gmail.com

\*University of Oviedo, campus universitario, 33203, Gijón, Spain

## ABSTRACT

Tempering temperatures ranging between 500 and 720°C were applied in order to analyse the relationship between steel microstructure and the deleterious effect of hydrogen on the fracture toughness of different CrMo and CrMoV steels. The influence of hydrogen on the fracture behaviour of the steel was investigated by means of fracture toughness tests using CT specimens thermally pre-charged with hydrogen gas.

First, the specimens were pre-charged with gaseous hydrogen in a pressurized reactor at 19.5MPa and 450°C for 21h and elasto-plastic fracture toughness tests were performed under different displacement rates. The amount of hydrogen accumulated in the steel was subsequently determined in order to justify the fracture toughness results obtained with the different steel grades. Finally, scanning electron microscopy was employed to study both the resulting steel microstructures and the fracture micromechanisms that took place during the fracture tests.

According to the results, hydrogen solubility was seen to decrease with increasing tempering temperature, due to the fact that hydrogen microstructural trapping is lower in relaxed martensitic microstructures, the strong effect of the presence of vanadium carbides also being noted in this same respect. Hydrogen embrittlement was also found to be much greater in the grades tempered at the lowest temperatures (with higher yield strength). Moreover, a change in the fracture micromechanism, from ductile (microvoid coalescence, MVC), in the absence of hydrogen, to intermediate (plasticity-related hydrogen induced cracking, PRHIC) and brittle (intergranular fracture, IG), was appreciated with the increase in the embrittlement indexes.

**KEYWORDS:** Hydrogen embrittlement, fracture toughness, quenched and tempered steels, thermally pre-charged specimens, failure micromechanisms.

## 1. INTRODUCTION

Hydrogen is considered a future alternative energy source to fossil fuels. Commercial fuel cell vehicles and hydrogen refueling stations are currently in construction in many countries. In such hydrogen infrastructures, different metallic components such as hydrogen tanks, pipes and valves are directly exposed to a high-pressure hydrogen gas environment. Under typical in-service hydrogen pressures of up to 70 MPa, it is well known that hydrogen can easily enter and diffuse into metals, thereby deteriorating their mechanical properties such as tensile strength, ductility, fracture toughness and fatigue crack propagation rate [1,2].

In general, hydrogen systems have typically been designed using alloys with a high resistance to hydrogen embrittlement, such as austenitic stainless steels and aluminium alloys. However, these metals have a lower strength and are more expensive than conventional structural steels, such as low-alloy steels [3, 4]. The best solution to this problem, based on the criteria of economy and performance, would be to use medium- and high-strength tempered martensitic steels, which allow decreasing pipe and vessel thicknesses and hence a lower cost of the steel.

Cr-Mo and Cr-Mo-V steels are frequently used in the quenched and tempered condition when a good combination of strength and toughness is required. They also have high fatigue strength, thus far being an excellent choice in the manufacture of vessels and pipes able to work under high-pressure hydrogen gas [5, 6]. Nevertheless, it is well known that high strength steels are more sensitive to hydrogen embrittlement (HE) than low-strength grades, this susceptibility increasing with the strength level of the steel [7, 8]. In order to overcome this drawback, they may be tempered at high temperatures, where their strength and hardness significantly decline, as was shown recently in [9], where the

application of a tempering treatment of 650° and 700°C during two hours gave rise to the best notched tensile behaviour when tested with internal hydrogen.

On the other hand, the susceptibility of structural materials to hydrogen-assisted fracture under high pressure hydrogen atmospheres can be assessed by (1) mechanical testing under high-pressure hydrogen gas (applying stress concurrent with hydrogen entrance), and (2) testing in air after pre-charging the specimens with hydrogen (applying stress following hydrogen exposure). These environmental conditions are referred to as external hydrogen and internal hydrogen, respectively [10]. In the case of external hydrogen, the measurement of mechanical properties under controlled hydrogen pressures requires the use of highly specialized facilities, as material test specimens may be exposed to high-pressure hydrogen gas while being subjected to specific mechanical loads.

Different authors [5, 11, 12] have determined the fracture toughness of steels under external hydrogen conditions at high hydrogen pressures. They have demonstrated that the application of hydrogen pressure causes a significant decrease in the toughness of steels and that this property also depends strongly on the applied loading rate. According to San Marchi and Sommerday [11], fracture toughness of 2.25Cr1Mo steel in hydrogen gas is significantly lower than the fracture toughness in argon and these differences are sensitive to yield strength and hydrogen pressure, increasing as yield strength and hydrogen pressure increase. It was also recognized that Cr-Mo steels with yield strengths lower than 750 MPa have demonstrated reliable performance in hydrogen services, with a lower bound fracture threshold in hydrogen gas of at least 50 MPam<sup>1/2</sup> [10]. On the other hand, using a low carbon non-alloyed steel (with a yield strength of 360MPa), Ogawa et al [13] reported significant fracture toughness degradation in 115 MPa hydrogen gas pressure, but only a slight degradation in 0.7 MPa hydrogen gas.

In contrast, the use of hydrogen pre-charged specimens is a readily available methodology and thermal pre-charging is a very convenient way to introduce controlled hydrogen contents into the samples. The thermal pre-charging method is relatively simple, as material test specimens are exposed to high-pressure hydrogen gas at a high temperature. In principle, the pressure and temperature are selected in accordance with the material and specimen dimensions so as to achieve a uniform hydrogen concentration in the specimen. In practice, uniform hydrogen concentrations can be achieved in conventional-sized specimens of structural steels within reasonable timeframes.

Pre-charging of specimens in hydrogen atmospheres may be limited to 450°C and 48 hours so as to completely avoid the methane reaction, which is the reaction between hydrogen atoms and solute carbon to produce a methane molecule [14]. With the aforementioned limitation, thermal pre-charging is able to produce samples with high hydrogen contents and uniform hydrogen distribution. However, hydrogen egress cannot be avoided during the cooling phase at the end of high temperature pre-charging until the extraction temperature is reached. Moreover, the final hydrogen concentration at room temperature is highly supersaturated, as hydrogen solubility depends exponentially on temperature [10].

Several studies on the effect of hydrogen on the fracture toughness of steels using thermally pre-charged specimens have also been performed. According to [14], the J crack growth initiation value, J<sub>0.2</sub>, respectively decreased from 600 to 60 kJ/m<sup>2</sup> and from 400 to 250 kJ/m<sup>2</sup> in CrMo and CrMoV steels, with this same parameter decreasing 5-fold between a loading rate of 0.3 mm/min and that of 0.005 mm/min. Similarly, Liu et al. [15] observed a drop in the fracture toughness of a ferritic SA508-III steel thermally precharged at 10MPa, as the hydrogen content introduced in the steel increased (different H contents were achieved changing the reactor temperature between 150 and 300°C). They also noticed a clear change in the fracture micromechanism from ductile microvoid coalescence (MVC) to a mixture fracture of dimples and cleavage facets.

Colombo et al. [16] reported a strong decrease in J<sub>IC</sub> for the onset of crack growth in a quenched and tempered 4130 (CrMo) steel, from 215 kJ/m<sup>2</sup> in air to 22 kJ/m<sup>2</sup> in the presence of internal hydrogen (in this case the steel was electrochemically pre-charged). The authors stated that this fracture toughness embrittlement index was comparable with those obtained by Loginow and Phelps [17] in a similar steel grade tested in gaseous hydrogen at very high pressure. A significant deleterious effect of the presence of internal hydrogen on the fracture toughness of a high strength API X90 pipeline steel (with a 640 MPa yield strength) was also reported by Li et al. [18] and such embrittlement was observed to increase with the thickness of the fracture specimen (higher constraint). Using also electrochemically hydrogen pre-charged specimens, Thomas et al. showed a very strong decrease of the plain-strain fracture toughness of an Aermet 100 steel (with a very high yield strength of 1765 MPa) from 143 MPam<sup>-1/2</sup> in air to 15

MPam<sup>-1/2</sup> with internal hydrogen, and fracture micromechanisms changed from ductile to transgranular cleavage [19]. Modifications of fracture micromechanisms from microvoid coalescence in air, to transgranular cleavage or even intergranular fracture with internal or external hydrogen, were also observed by many researchers [13, 14, 15, 20, 21].

Anyway, there is now a need for wider-ranging research programs on this topic, and the use of thermally pre-charged specimens is very convenient for this purpose. Hydrogen pre-charged specimens were used in the present study to elucidate the effects of hydrogen on the fracture toughness of 42CrMo4, 2.25Cr1Mo and 2.25Cr1MoV steels, quenched and tempered at different temperatures, in order to obtain grades with different yield strengths. Furthermore, the effect of employing different displacement rates was also investigated.

## 2. EXPERIMENTAL PROCEDURE

### 2.1 Materials and heat treatments

Two CrMo and a CrMoV steels with the chemical compositions in weight % shown in Table 1 were used in this study.

Table 1. Chemical compositions of CrMo and CrMoV steels (wt. %).

Steel	C	Mn	Si	P	S	Cr	Mo	V
42CrMo4	0.42	0.62	0.18	0.008	0.002	0.98	0.22	---
2.25Cr1Mo	0.14	0.56	0.16	0.005	0.002	2.23	1	---
2.25Cr1MoV	0.15	0.52	0.09	0.006	0.002	2.27	1.1	0.31

Hot rolled plates (12 mm thick) of 42CrMo4 were austenitized at 845°C for 40 min, quenched in water, and then tempered at 5 different temperatures between 500 and 700°C, for 2 hours. In addition, 2.25Cr1Mo and 2.25Cr1MoV steels were also respectively water quenched from 940 and 925°C and then tempered at the temperatures and times shown in Table 2. The reason for using different heat treatments was to obtain different steel grades so as to analyse the way hydrogen degrades the fracture toughness of one and the same steel but with different microstructures and strength levels.

Table 2. Heat treatments applied to CrMo and CrMoV steels.

Steel grade	Heat treatments
42CrMo4_700	845°C/40min + water quenching + 700°C/2h tempering
42CrMo4_650	845°C/40min + water quenching + 650°C/2h tempering
42CrMo4_600	845°C/40min + water quenching + 600°C/2h tempering
42CrMo4_550	845°C/40min + water quenching + 550°C/2h tempering
42CrMo4_500	845°C/40min + water quenching + 500°C/2h tempering
2.25Cr1Mo_690	940°C/30min + water quenching + 690°C/30h tempering
2.25Cr1Mo_600	940°C/30min + water quenching + 600°C/2h tempering
2.25Cr1MoV_720	925°C/30min + water quenching + 720°C/3h tempering
2.25Cr1MoV_650	925°C/30min + water quenching + 650°C/2h tempering

### 2.2 Hydrogen charging

All the specimens were pre-charged with gaseous hydrogen in a high-pressure reactor and were kept in contact with gaseous hydrogen under a pressure of 19.5 MPa at 450°C for 21 h. After this holding time, the reactor was allowed to cool for 1h until reaching a temperature of 85°C. During this phase, the hydrogen pressure was maintained constant at 19.5 MPa to reduce hydrogen egress. All the pre-charged specimens were subsequently removed from the reactor and immersed in liquid nitrogen (-196°C), where they were kept until the start of the corresponding test, once again in order to limit hydrogen losses.

### 2.3 Measurement of hydrogen content

The hydrogen content in the specimens was measured by means of thermal desorption analysis (TDA) using a Leco DH603 hydrogen analyser. The equipment's measurement principle is based on the difference in thermal conductivity between a reference gas flow of pure nitrogen and a secondary flow composed of nitrogen and the hydrogen thermally extracted from the sample kept at 1100°C for 400s. Cylindrical steel pins of 10 mm in diameter and 30 mm long ( $\approx 20$ g) were used for this purpose. After extraction from the liquid nitrogen and before the measurement, each pin was cleaned in an ultrasonic bath with acetone for 5 minutes and carefully dried using cold air. Hydrogen content measurements were performed just after pre-charging, so as to determine the total hydrogen introduced into the steels, and after 5 days at room temperature to determine the strongly trapped hydrogen.

#### 2.4 Fracture toughness tests

Fracture toughness characterization was performed using compact test (CT) specimens with a width  $W=48$  mm, a thickness  $B=12$  mm, and an initial notch  $a_n=20$ mm. First, the specimens were fatigue pre-cracked at  $R=0.1$  and  $f=10$ Hz, until obtaining a crack length versus width ratio,  $a/W=0.5$ , following the ASTM E1820 standard [22]. Lateral notches were then machined on both sides of the specimen until reaching a net thickness,  $B_n=10$ mm, so as to ensure a plane strain state.

Fracture toughness tests without hydrogen were carried out under a nominal displacement rate of 1 mm/min. Hydrogen pre-charged specimens were tested under displacement rates of 1, 0.1, 0.01 and 0.001mm/min (also depending on the steel grade) in order to study the influence of this parameter on HE.

Crack growth in the course of the tests was determined by means of the compliance method, carrying out 25% partial discharges using a CTOD gauge. The initial and final crack lengths were corrected by measuring them on the fracture surface of the broken specimen. The J value obtained in each discharge was calculated as the sum of its elastic and plastic components. The former was calculated from the stress intensity factor, K, while the latter was obtained by integrating the area below the load-displacement plot.

The fracture toughness initiation parameter  $J_{0.2/BL}$  (kJ/m<sup>2</sup>) was used. This parameter corresponds to the value of J after a crack growth of 0.2 mm offset to the blunting line. Furthermore, in order to assess the effects of hydrogen in the crack propagation stage, the  $J_{1.2/BL}$  parameter (J value corresponding to a crack propagation of 1.2 mm) was also considered.

It should be noted that due to the high brittleness of the 42CrMo4 steel grades tempered at 550 and 500°C, it was not possible to determine the value of  $J_{0.2/BL}$  when these steels were tested with internal hydrogen under low displacement rates. Therefore, the value of  $P_Q$  for these steel grades was calculated from the Load-CTOD curve,  $P_Q$  being the load obtained on the plot when decreasing the slope of the linear elastic line 5%. This value was then used to estimate the  $K_Q$  and  $J_Q$  parameters following the specifications of the standard [22].

Finally, the decrease in fracture toughness caused by the presence of internal hydrogen was defined by means of the embrittlement index (EI), defined in Eq. (1) (EI varies from 0, no embrittlement at all, to 100%, maximum possible hydrogen embrittlement).

$$EI [\%] = \frac{X - X_H}{X} \cdot 100 \quad (1)$$

where X and  $X_H$  are respectively the measured toughness property evaluated without and with internal hydrogen.

#### 2.5 Observation of microstructures and fracture surfaces

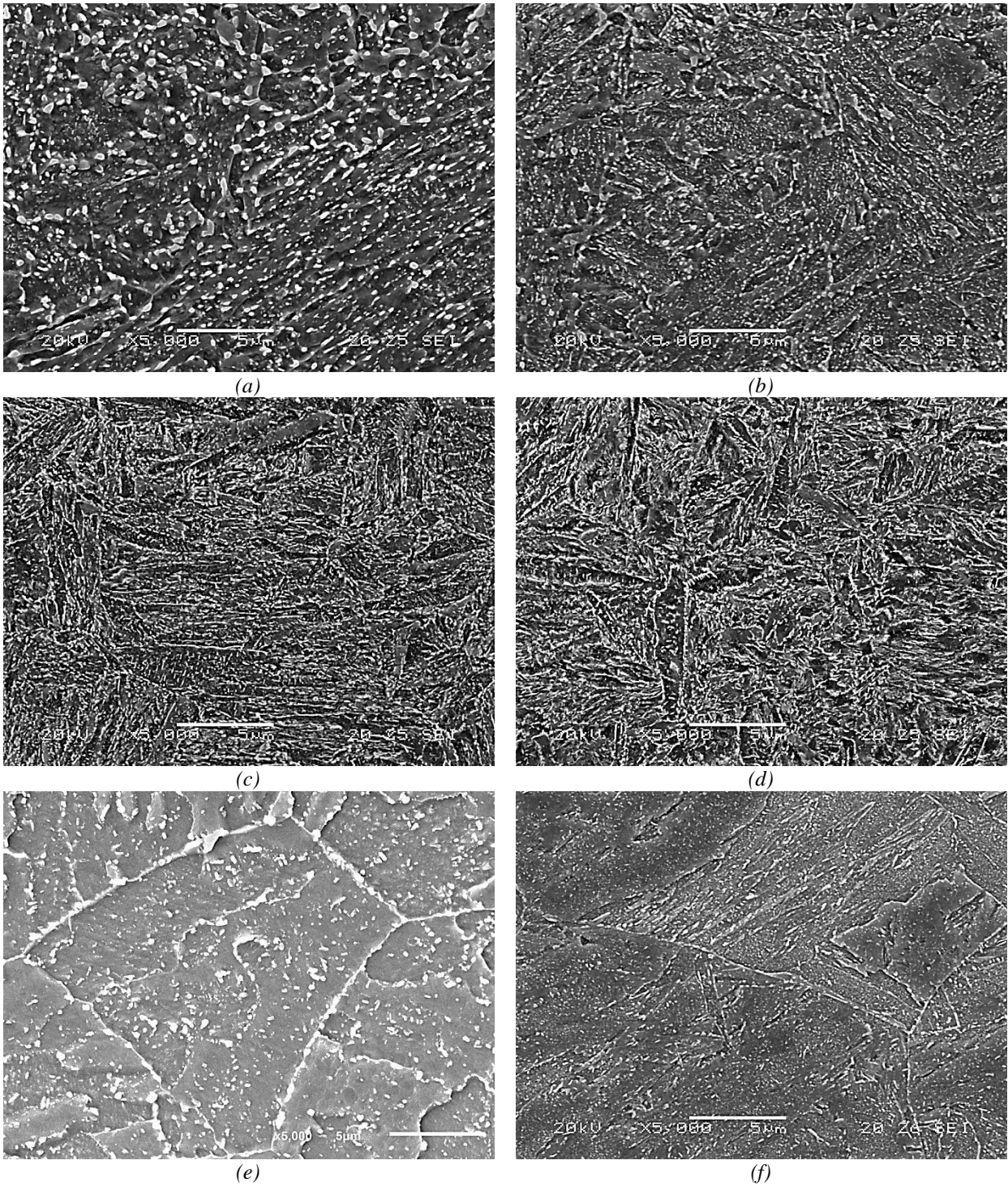
The microstructures obtained after the application of the different heat treatments were observed by means of a scanning electron microscope (SEM JEOL-JSM5600) under an acceleration voltage of 20 kV. The samples were ground, polished with diamond paste and finally etched with Nital-2%.

The fracture surfaces of the tested specimens were also analysed using the same scanning electron microscope under different magnifications.

### 3. RESULTS

### 3.1 Steel microstructures

The SEM microstructures of some of the 42CrMo steel grades are shown in Fig. 1, along with the microstructures of the 2.25Cr1Mo and 2.25Cr1MoV steels obtained after applying the aforementioned thermal treatments.



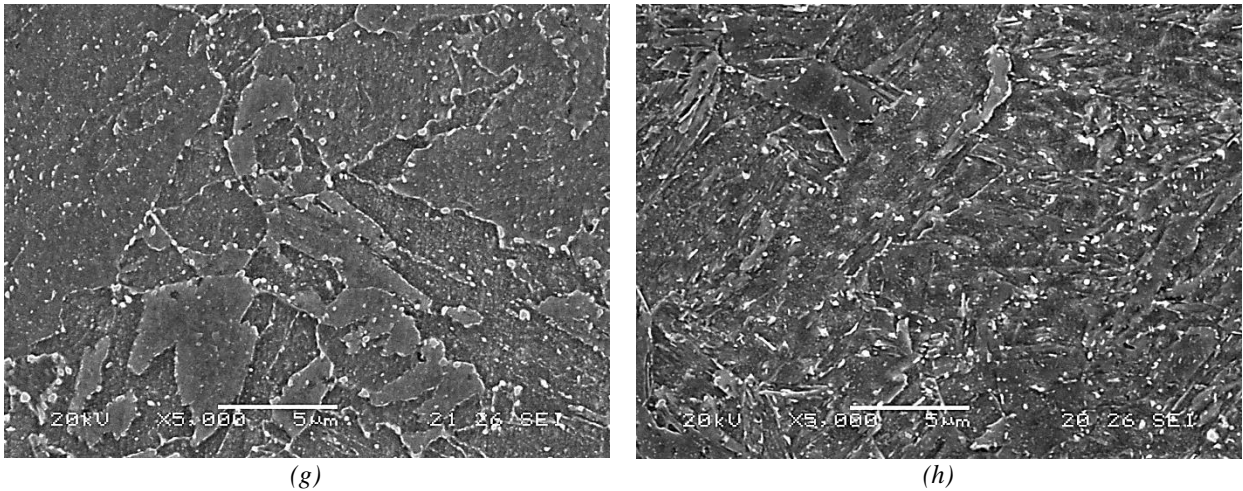


Figure 1. SEM microstructures of (a) 42CrMo4\_700, (b) 42CrMo4\_650, (c) 42CrMo4\_600, (d) 42CrMo4\_500, (e) 2.25Cr1Mo\_690, (f) 2.25Cr1Mo\_600, (g) 2.25Cr1MoV\_720 and (h) 2.25Cr1MoV\_650.

The obtained microstructure was in all cases tempered martensite, in which the profuse carbide precipitation that takes place during the tempering process can be clearly seen. Martensite internal residual stresses relax, dislocation rearrangement/annihilation and substructure recovery takes place, elongated carbides first precipitated in martensite block and packet boundaries break up, globulize and finally grow to yield a more uniform distribution with increasing tempering temperature [23]. Just as an example, compare the microstructures of 42CrMo4 steel quenched and tempered at 500°C (Fig. 1(d)) and 700°C (Fig. 1(a)). After tempering at 700°C, carbides have larger size, a more spherical morphology and are distributed in a more uniform way.

The aforementioned microstructural differences give rise to the hardness and tensile properties listed in Table 3. As expected, yield strength,  $\sigma_{ys}$ , ultimate tensile strength,  $\sigma_{uts}$  and Brinell hardness, HB, progressively decrease with increasing tempering temperature, while the opposite occurs with tensile elongation, e, and reduction in area, RA.

Table 3. Tensile properties and Brinell hardness (HB) of the different CrMo and CrMoV grades.

Steel Grades	Heat treatment	$\sigma_{ys}$ [MPa]	$\sigma_{uts}$ [MPa]	e [%]	RA [%]	HB
42CrMo4_700	845°C+WQ+T700°C/2h	622	710	22	61	201
42CrMo4_650	845°C+WQ+T650°C/2h	820	905	16	57	246
42CrMo4_600	845°C+WQ+T600°C/2h	880	985	15	55	281
42CrMo4_550	845°C+WQ+T550°C/2h	1023	1113	14	49	307
42CrMo4_500	845°C+WQ+T500°C/2h	1086	1198	13	51	335
2.25Cr1Mo_690	940°C+WQ+T690°C/30h	430	580	27	72	170
2.25Cr1Mo_600	940°C+WQ+T600°C/2h	761	887	19	75	285
2.25Cr1MoV_720	925°C+WQ+T720°C/3h	567	714	20	80	200
2.25Cr1MoV_650	925°C+WQ+T650°C/2h	667	829	20	75	262

Note also that steel grades with yield strengths between 430 and 1086 MPa were produced. It is well known that hydrogen embrittlement increases with the strength level of the steel [5-9]; hence grades tempered at lower temperatures are expected to be more susceptible to HE.

### 3.2 Hydrogen uptake

All the hydrogen values measured in the different CrMo and CrMoV steel grades are shown in Table 4. The initial hydrogen content after thermal pre-charging,  $C_{H0}$ , and the final hydrogen content,  $C_{HF}$ , i.e. hydrogen strongly trapped and retained in the steel microstructure after a long time at room temperature (around five days in our tests) were determined. The difference between these two values is the diffusible hydrogen, i.e. weakly and reversibly trapped hydrogen able to move through the steel microstructure. An initial hydrogen content of between 0.6 and 1.9 ppm was

introduced in the different CrMo steel grades. Moreover, the final hydrogen content is even more dependent on the microstructure of the steel than the former value, decreasing as the tempering temperature increases, mainly due to stress relaxation and the reduction in dislocation density and internal interphases (martensite blocks and packets). On the other hand, CrMoV steel grades were able to absorb much larger hydrogen values due to the presence of very fine vanadium carbides [14, 24, 25] that were strongly trapped in their microstructures. In this case, tempering at a higher temperature slightly increases the hydrogen trapping capacity of the steel, mainly due to differences in vanadium carbide precipitation, size and distribution.

Table 4. Initial ( $C_{H0}$ ), final ( $C_{Hf}$ ) and diffusible hydrogen ( $C_{H0}-C_{Hf}$ ) measured in the different CrMo and CrMoV steel grades.

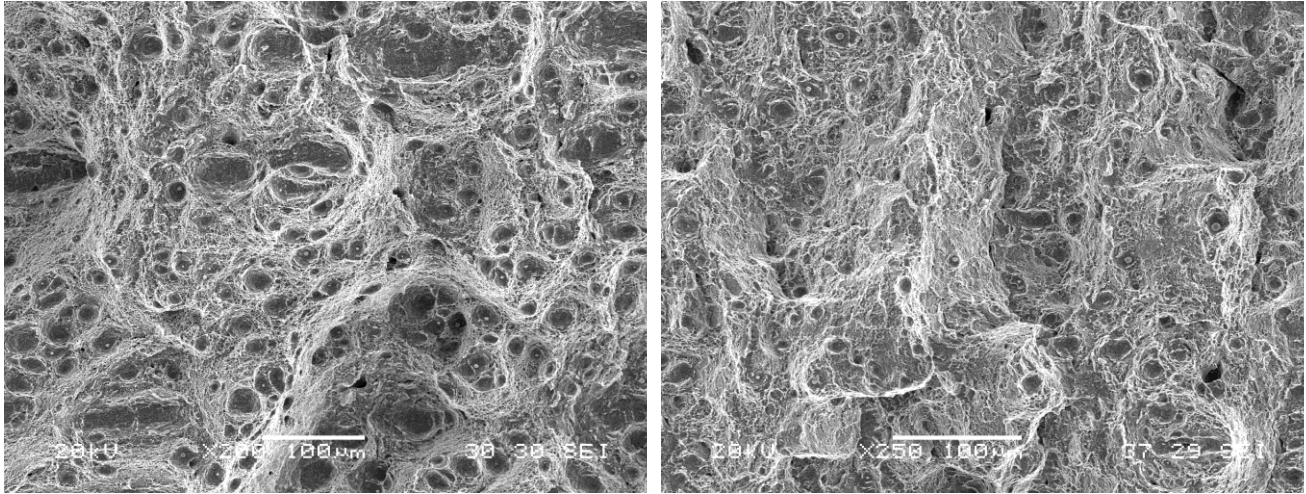
Steel Grades	HB	$C_{H0}$ [ppm]	$C_{Hf}$ [ppm]	$C_{H0}-C_{Hf}$ [ppm]
42CrMo4_700	201	1.2	0.4	0.8
42CrMo4_650	246	1.2	0.7	0.5
42CrMo4_600	281	1.4	0.9	0.5
42CrMo4_550	307	1.7	1.4	0.3
42CrMo4_500	335	1.9	1.7	0.2
2.25Cr1Mo_690	170	0.6	0.2	0.4
2.25Cr1Mo_600	285	1.3	0.6	0.7
2.25Cr1MoV_720	200	4.3	3.9	0.4
2.25Cr1MoV_650	262	3.8	3.4	0.4

### 3.3 Fracture toughness

Fracture toughness results with respect to the steel grades tested without hydrogen are shown in Table 5. The potential law from the fitted experimental data,  $J=C_1\Delta a^{C_2}$ , is also included in this table and allows us to estimate the J value for any value of crack growth. As expected, the value of  $J_{0.2/BL}$  (J crack growth initiation value determined for a 0.2 mm crack growth offset to the blunting line) decreases with decreasing tempering temperature (higher yield strength and ultimate tensile strength), as does the  $C_2$  parameter, which leads to a flatter crack propagation curve. In all cases, the operative fracture micromechanism was fully ductile microvoid coalescence (MVC), as can be seen in Fig. 2 for the 42CrMo4 specimens respectively tempered at the highest and lowest temperatures, 700 and 500°C.

Table 5. Elasto-plastic fracture toughness results. CrMo and CrMoV steel grades. Uncharged specimens.

Steel Grade	$\sigma_{ys}$ [MPa]	$\sigma_{uts}$ [MPa]	$J_{0.2/BL}$ [kJ/m <sup>2</sup> ]	$J=C_1\Delta a^{C_2}$	
				$C_1$	$C_2$
42CrMo4_700	622	710	580	739	0.54
42CrMo4_650	820	905	396	670	0.62
42CrMo4_600	880	985	292	456	0.43
42CrMo4_550	1023	1113	280	455	0.48
42CrMo4_500	1086	1198	249	369	0.33
2.25Cr1Mo_690	430	580	904	867	0.60
2.25Cr1Mo_600	761	887	743	941	0.54
2.25Cr1MoV_720	567	714	672	847	0.71
2.25Cr1MoV_650	667	829	533	767	0.62



(a) (b)  
 Figure 2. Fracture surfaces on uncharged CT specimens of (a) 42CrMo4\_700 and (b) 42CrMo4\_500.

Tables 6 and 7 show the results of all the fracture toughness tests carried out on uncharged and on hydrogen pre-charged specimens under different displacement rates. Additionally, the required J value for the initial crack to grow 1 mm, from 0.2 to 1.2 mm,  $\Delta J_{0.2 \rightarrow 1.2/BL}$ , the embrittlement indexes and the operative fracture micromechanisms (by order of importance) are also given.

Table 6. Results of fracture toughness tests performed on the 42CrMo4 steel grade, uncharged and hydrogen pre-charged, loaded at different displacement rates ( $J_Q = K_Q^2(1 - \nu^2)/E$ ). \*MVC: microvoid coalescence; PRHC: plasticity-related hydrogen induced cracking; IG: intergranular (in order of importance).

Steel Grade	$V_{test}$ [mm/min]	$J_{0.2/BL}$ [kJ/m <sup>2</sup> ]	$J_{1.2/BL}$ [kJ/m <sup>2</sup> ]	$\Delta J_{0.2 \rightarrow 1.2/BL}$ [kJ/m <sup>2</sup> ]	EI( $J_{0.2/BL}$ ) [%]	EI( $\Delta J_{0.2 \rightarrow 1.2/BL}$ ) [%]	*Fracture Micromechanisms	
42CrMo4	700	1.00	580	1073	493	-	-	MVC
		1.00	350	724	374	40	24	MVC+PRHC
		0.10	380	757	377	34	24	MVC+PRHC
		0.01	345	585	240	41	51	MVC+PRHC
	650	1.00	396	950	454	-	-	MVC
		1.00	303	600	297	23	35	MVC+PRHC
		0.10	273	560	287	31	37	MVC+PRHC
		0.01	249	505	256	37	44	PRHC
	600	1.00	292	545	253	-	-	MVC
		1.00	205	340	135	30	47	MVC+PRHC
		0.10	191	260	69	35	73	MVC+PRHC+IG
		0.01	53	120	67	82	74	PRHC+IG
	$T_{rev}$	$V_{test}$ [mm/min]	$P_Q$ [N]	$K_Q$ [MPam <sup>-1/2</sup> ]	$J_Q$ [kJ/m <sup>2</sup> ]	EI( $P_Q$ ) [%]	EI( $J_Q$ ) [%]	*Fracture Micromechanisms
	550	0.100	30750	143	89	-	-	MVC
		0.100	22404	107	50	37	44	MVC+PRHC+IG
		0.010	12500	66	19	59	79	PRHC+IG+MVC
0.001		8900	43	8	71	91	IG+PRHC	
500	0.100	41892	157	112	-	-	MVC	
	0.100	23262	85	32	45	71	MVC+IG+PRHC	
	0.010	12611	43	8	70	93	IG+PRHC	
	0.001	7416	17	1	82	99	IG+PRHC	

Table 7. Results of fracture toughness tests performed on the 2.25Cr1Mo and 2.25Cr1MoV steel grades, uncharged and hydrogen pre-charged, loaded at different displacement rates. \*MVC: microvoid coalescence; PRHIC: plasticity-related hydrogen induced cracking; IG: intergranular (in order of importance).

Steel Grade	$V_{\text{test}}$ [mm/min]	$J_{0.2/BL}$ [kJ/m <sup>2</sup> ]	$J_{1.2/BL}$ [kJ/m <sup>2</sup> ]	$\Delta J_{0.2 \rightarrow 1.2/BL}$ [kJ/m <sup>2</sup> ]	EI( $J_{0.2/BL}$ ) [%]	EI( $\Delta J_{0.2 \rightarrow 1.2/BL}$ ) [%]	*Fracture Micromechanisms	
2.25Cr1Mo	690	1.00	904	1560	656	-	-	MVC
		1.00	502	1062	560	43	15	MVC+PRHIC
		0.10	602	1240	638	33	3	MVC+PRHIC
		0.01	465	701	236	49	64	MVC+PRHIC
	600	1.00	743	1410	667	-	-	MVC
		1.00	389	786	397	47	40	MVC
		0.10	394	680	286	47	57	MVC+PRHIC
		0.01	294	584	290	60	57	PRHIC+IG
2.25Cr1MoV	720	1.00	672	1600	928	-	-	MVC
		1.00	542	1280	738	19	20	MVC
		0.10	420	880	460	38	54	MVC
		0.01	448	784	336	37	64	MVC
	650	1.00	533	1188	655	-	-	MVC
		1.00	403	660	257	24	61	MVC
		0.10	341	637	296	36	57	MVC
		0.01	314	580	266	41	59	MVC

The fracture toughness-crack growth ( $J$ - $\Delta a$ ) curves of the 42CrMo4 grade tempered at the highest temperature (700°C) with the lowest yield strength, corresponding to uncharged and H-charged specimens, at 1, 0.1 and 0.01mm/min, are shown in Fig. 3. The effect of hydrogen is noticeable in all cases, giving rise to a clear decrease in  $J_{0.2/BL}$  and  $J_{1.2/BL}$ . Maximum embrittlement occurred under the lowest displacement rate, 0.01 mm/min. However, a decrease in fracture toughness when decreasing the displacement rate was noted in all the tested grades (see Tables 6 and 7), as the accumulation of hydrogen atoms in the process zone located ahead of the crack tip of the CT fracture specimen (trapped by dislocations in the plastic zone and also driven by the high hydrostatic stress existing at the crack front) increases due to the availability of longer diffusion times, giving rise to the embrittlement phenomenon. It is well known that mobile hydrogen atoms move due to being attracted by local hydrostatic stress,  $\sigma_h$ , which according to continuum plasticity theory reaches a maximum at a distance  $x$  from the crack tip,  $x=J/\sigma_{ys}$ . Moreover, local strain exhibits a singularity at the crack tip, reaching very high values ( $\epsilon_{eq}>10\%$ ) at approximately half this distance ( $J/2\sigma_{ys}$ ), where the dislocation density multiplies, giving rise to high local hydrogen accumulation [26, 27].

The fracture surface of the specimen tested under the lowest displacement rate can be seen in Fig. 4(a). Two different regions can be distinguished: Region 1, with an extension of between 250-300 $\mu\text{m}$ , corresponds to the crack initiation phase, while Region 2 corresponds to the propagation phase. Taking into account the values of  $J_{0.2/BL}$  measured in this specimen (345 kJ/m<sup>2</sup>) and the yield strength of this steel (622 MPa), the extension of the strained region where hydrogen accumulates is 280  $\mu\text{m}$ . Region 1, which can be seen in more detail in Fig. 4(b), exhibits the appearance of a transgranular fracture surface or quasi-cleavage, usually referred to as plasticity-related hydrogen induced cracking (PRHIC) in martensitic steels [28]. The PRHIC mechanism was first described by Takeda and McMahon [29] in reference to the fracture mechanism observed in a low alloy quenched and tempered steel in hydrogen gas. It is sometimes called tearing topography surface or TTS, which is described as a fracture surface characterised by ductile micro-plastic tearing on a very fine scale, along martensite block and packet interphases [28, 30]. The size of the characteristic features observed in Fig. 4(b) is comparable to the microstructure units (martensite blocks and packets); hence, hydrogen accumulation promotes plastic deformation and final decohesion of these interphases (HEDE, hydrogen-enhanced decohesion). A mixed micromechanism is observed in Region 2 (Fig. 4(a)), with areas of MVC and PRHIC, in the latter case inside the expanded microvoids caused by a local increase in plasticity due to solute hydrogen, which facilitates the movement of dislocations (hydrogen-enhanced localized plasticity, HELP) [10, 31]. As the applied  $J$  increases, the plastic zone extends, diffusible hydrogen redistributes into a larger volume and hence, the total local

hydrogen content in the process zone decreases and PRHIC is no longer the only failure micromechanism (MVC also appears).

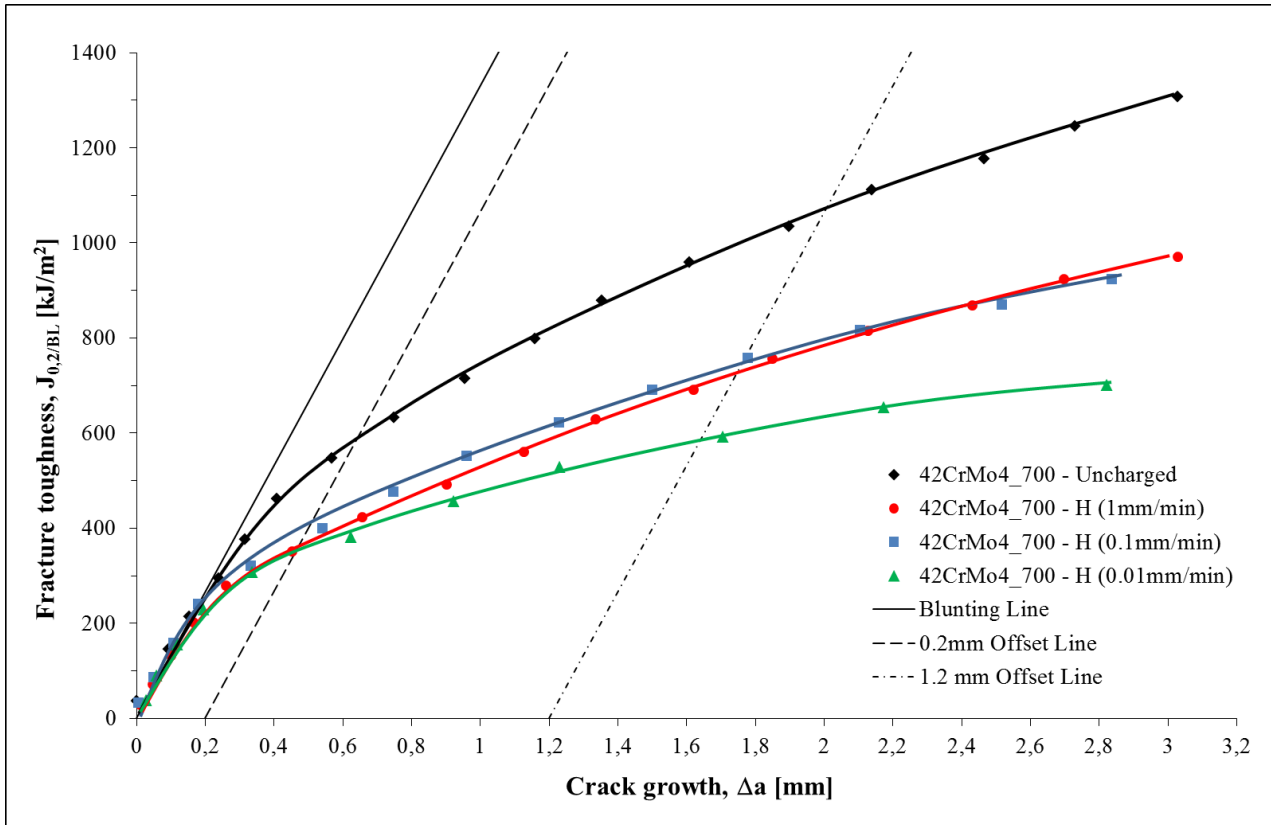


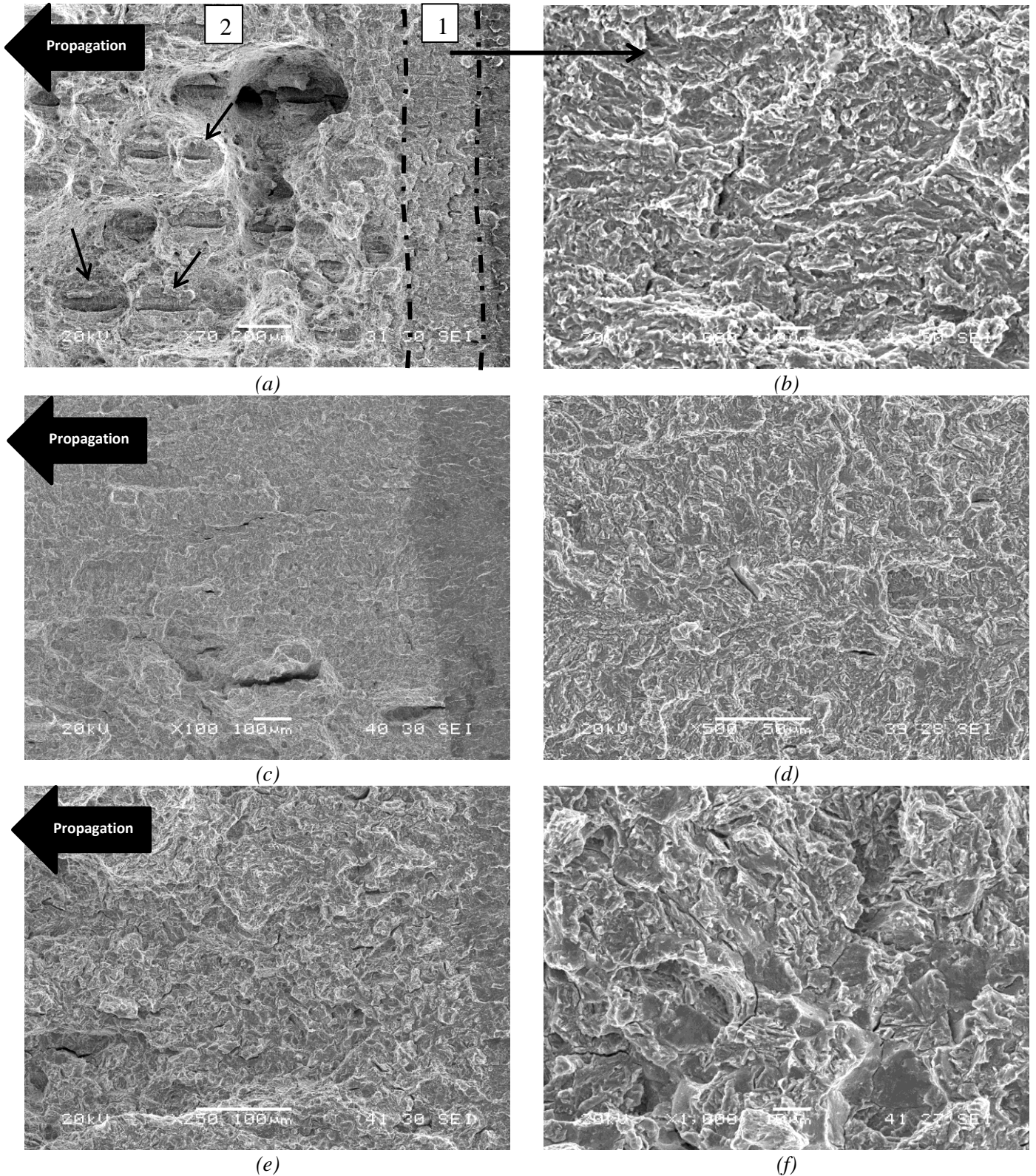
Figure 3.  $J$ - $\Delta a$  curves of uncharged and H-charged specimens of 42CrMo4\_700 grade.

The embrittlement indexes and predominant fracture micromechanisms corresponding to the steel grade quenched and tempered at 650°C for the different displacement rates, also shown in Table 6, are not so different from those observed in the 700°C tempered grade. As can be seen in Fig. 4(c) and (d), the fracture micromechanisms evolved from a fully ductile mechanism (MVC), in the absence of hydrogen, to PRHIC, when tested under internal hydrogen at the lowest displacement rate. Mixtures of MVC and PRHIC micromechanisms were observed in hydrogen pre-charged specimens tested at intermediate displacement rates (Table 6), as the available time for hydrogen diffusion decreased and hydrogen accumulation within the process zones was lower.

The hydrogen pre-charged steel grade quenched and tempered at 600°C tested at 0.1 mm/min already shows traces of IG fracture that finally, when tested at an even lower displacement rate, gives rise to a mixture of PRHIC and IG, as can be seen in Fig. 4(e) and (f). The higher initial and final hydrogen contents measured in this grade (Table 4), along with its higher yield strength ( $\sigma_h \sim 2.5\sigma_{ys}$ , according to continuum plasticity theory), provides greater hydrogen accumulation within the process zone, thus explaining this behaviour.

Finally, the extreme brittleness of the H-charged 42CrMo4 steel grades quenched and tempered at the lowest temperatures (550 and 500°C) precluded obtaining  $J$ - $\Delta a$  curves, so  $K_Q$  at instability (maximum load,  $P_Q$ ) was used as a characteristic fracture toughness parameter. The Load-COD displacement curves of the steel grade quenched and tempered at the lowest temperature, 500°C, are plotted in Fig. 5(a). In the test carried out at 0.001mm/min, the deleterious effects of hydrogen are noteworthy: the load,  $P_Q$ , drops over 80% and the embrittlement index relative to  $J_Q$  is practically equal to 100%. With regard to the fracture surfaces, as the displacement rate decreases, a clear evolution can be appreciated in the fracture micromechanisms. In this case, starting from MVC for the uncharged specimen, they pass through a mixture of MVC, PRHIC and IG for the charged specimen tested at 0.1mm/min to finish in a micromechanism mainly composed of IG fracture, with faint remnants of PRHIC features, for the lowest displacement rate, as can be observed in Fig. 4(i) and (j). Quite similar results were also obtained with the steel grade quenched and

tempered at 550°C (Fig. 5(b)): in the case of the test performed at the lowest displacement rate, the predominant micromechanism is IG, with isolated regions of PRHIC, Fig. 4 (g) and (h). These two grades have much higher levels of strongly trapped hydrogen than the other 42CrMo4 grades and also higher yield strengths (Tables 3 and 4). As mobile hydrogen accumulates in the process zone ahead of the crack tip submitted to high hydrostatic stress, attaining a concentration related to the steel yield strength ( $\sigma_h \sim 2.5\sigma_{ys}$ ), internal interphases such as prior austenitic grain joints and block and packet martensite boundaries easily fail under a relatively small local opening stress (HEDE micromechanism).



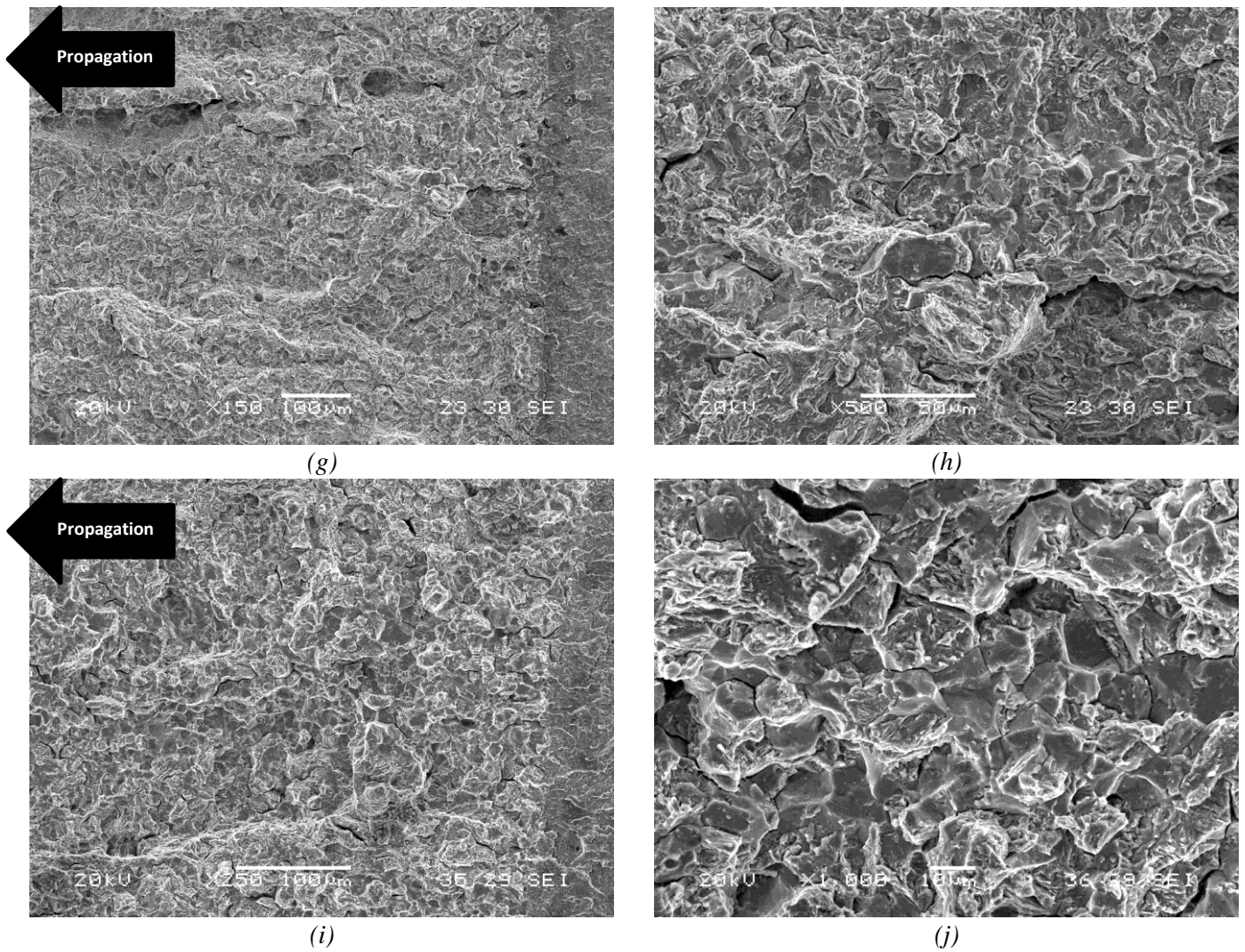


Figure 4. Fracture micromechanisms of 42CrMo4 grades tested with internal hydrogen at the lowest displacement rates. (a) 42CrMo4\_700 (0.01mm/min), (b) 42CrMo4\_700 (0.01mm/min), (c) 42CrMo4\_650 (0.01mm/min), (d) 42CrMo4\_650 (0.01mm/min), (e) 42CrMo4\_600 (0.01mm/min), (f) 42CrMo4\_600 (0.01mm/min), (g) 42CrMo4\_550 (0.001mm/min), (h) 42CrMo4\_550 (0.001mm/min), (i) 42CrMo4\_500 (0.001mm/min), (j) 42CrMo4\_500 (0.001mm/min)

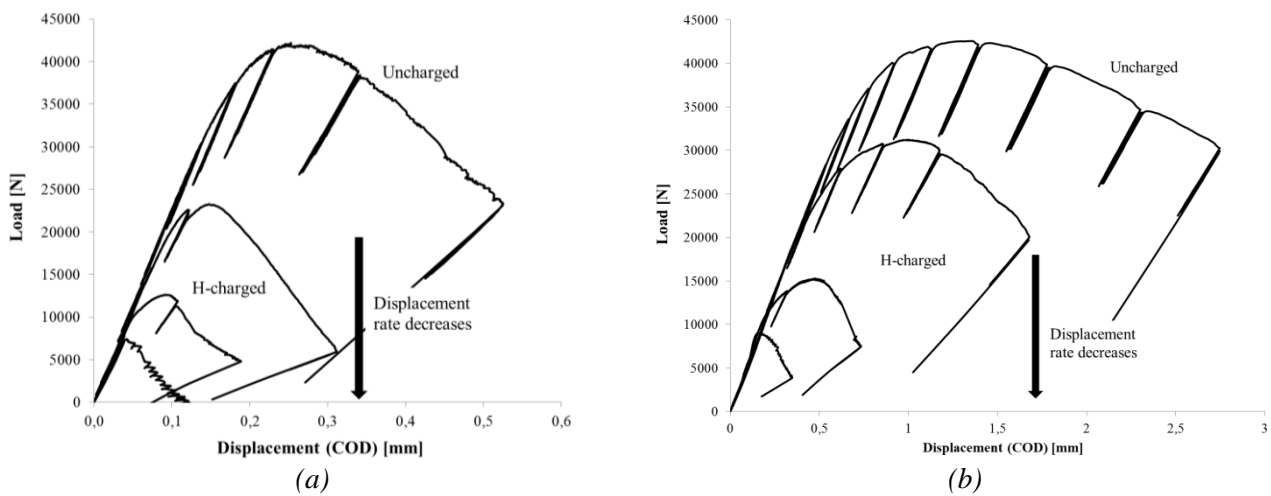
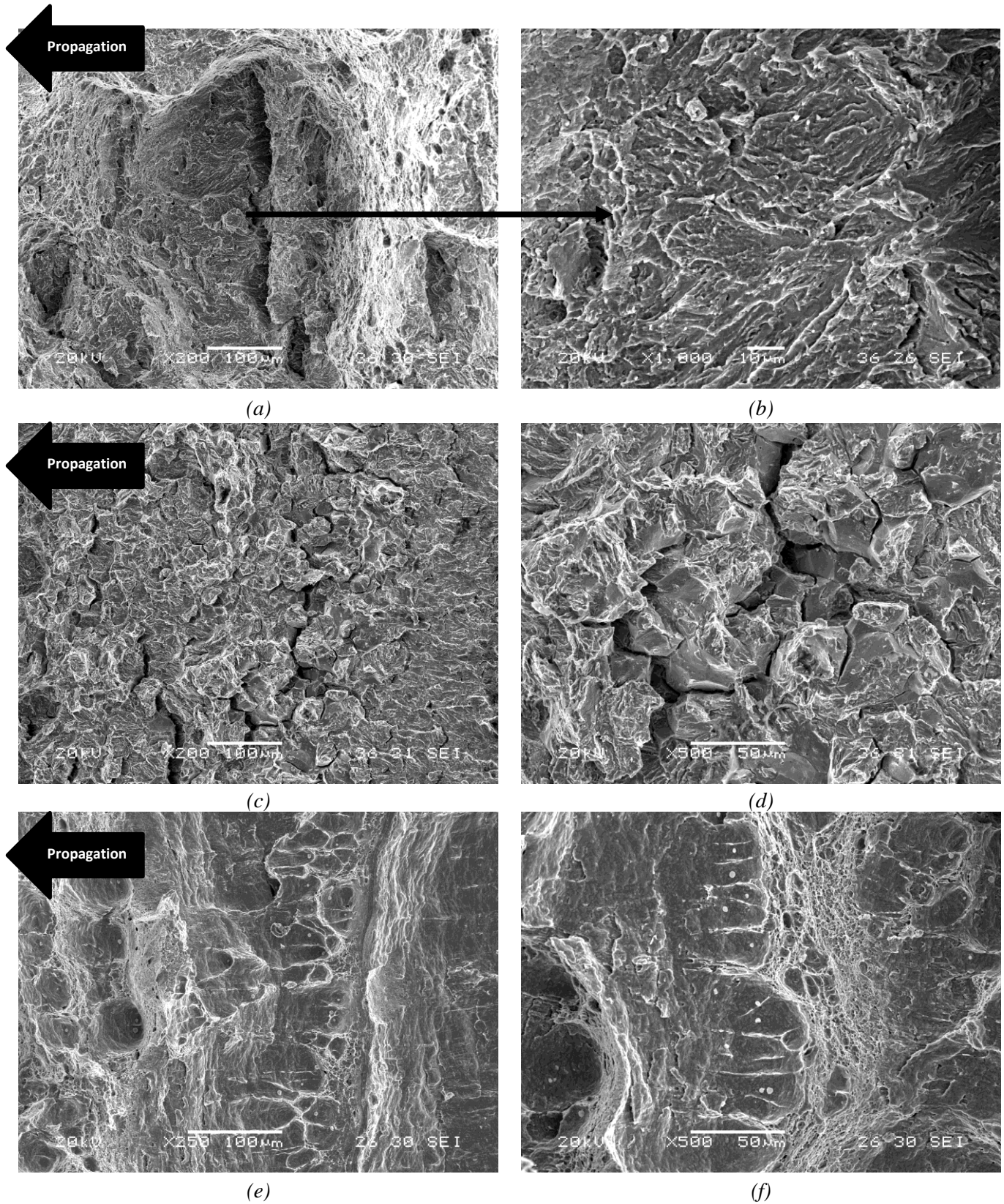
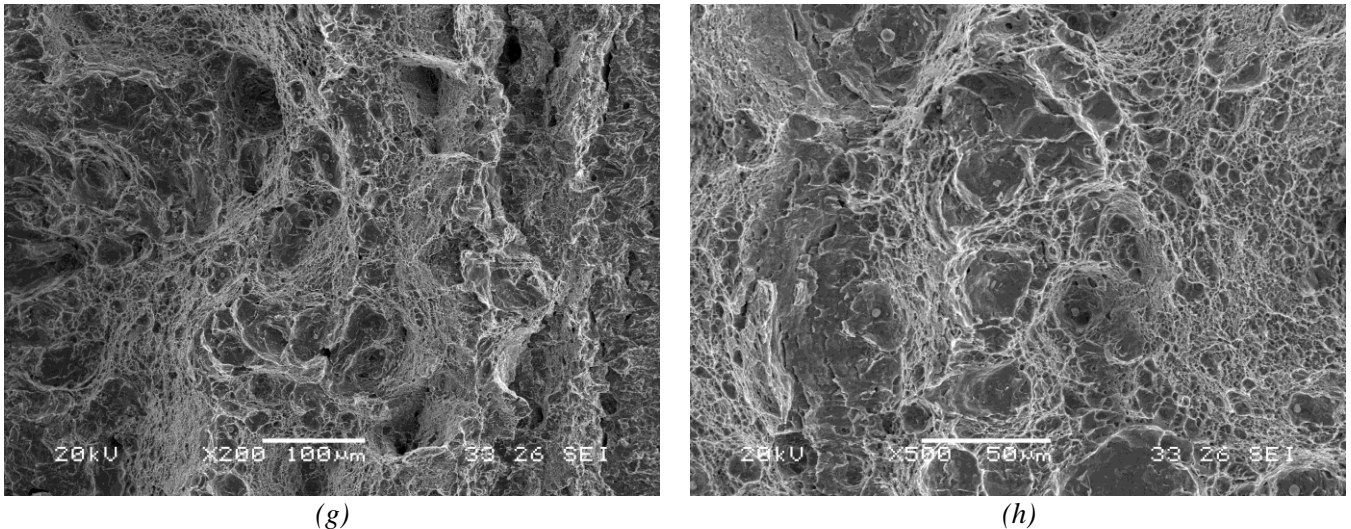


Figure 5. Load – Displacement (COD) curves corresponding to the 42CrMo4 steel quenched and tempered at (a) 500°C and (b) 550°C. Uncharged specimen and H-charged specimens tested at 0.1, 0.01 and 0.001mm/min.

The fracture surface of the quenched and tempered 2.25Cr1Mo and 2.25Cr1MoV specimens tested under internal hydrogen at the lowest displacement rate can be seen in Fig. 6. The fracture micromechanisms in 2.25Cr1Mo steel

tested with internal hydrogen resemble those already mentioned with respect to 42CrMo4 steel, with PRHIC and even some intergranular features (interphase decohesion) detected under the lowest displacement rates. Nevertheless, a unique and fully ductile fracture micromechanism (microvoid coalescence) is worth noting in all the fracture toughness tests performed with the 2.25Cr1MoV grade.





(g) (h)  
 Figure 6. Fracture micromechanisms of 2.25Cr1Mo and 2.25Cr1MoV steel grades tested with internal hydrogen at the lowest displacement rate, 0.01mm/min. (a) 2.25Cr1Mo\_690, (b) 2.25Cr1Mo\_690, (c) 2.25Cr1Mo\_600, (d) 2.25Cr1Mo\_600, (e) 2.25Cr1MoV\_720, (f) 2.25Cr1MoV\_720, (g) 2.25Cr1MoV\_650 and (h) 2.25Cr1MoV\_650.

#### 4. Selection of steels to be exposed to high-pressure hydrogen gas

Fig. 7 represents the critical stress intensity factor ( $J_{0.2/BL}$  or  $J_Q$ ) for the onset of crack growth under internal hydrogen and a displacement rate of 0.01 mm/min versus the steel yield strength for the 42CrMo4 steel grades. The predominant fracture micromechanisms are also shown in this figure. The sudden drop in fracture toughness under internal hydrogen and a low displacement rate when intergranular failure micromechanism appears (steel grade quenched and tempered at 600°C,  $\sigma_{ys} = 880$  MPa) are worth noting. As can be seen in Fig. 1(c), the Q+T microstructure of this steel still shows elongated carbides precipitated along prior austenite grain boundaries and packet and block martensite boundaries, resembling low tempering microstructures. These distorted internal interphases are able to trap and retain hydrogen (0.9 ppm H is strongly trapped, as can be seen in Table 4). Additionally, diffusible hydrogen (0.5 ppm) moves and accumulates in the process zone ahead of the crack tip of the CT specimen (within the plastic zone with a high dislocation density and at the maximum hydrostatic stress region) giving rise to a HEDE failure micromechanism (hydrogen-enhanced decohesion, PRHIC and IG). However, 42CrMo4 steel quenched and tempered at 650 and 700°C already has sufficiently relaxed Q+T microstructures with quite uniform dispersion of globular carbides (see Fig. 1(a) and (b)), so hydrogen distributes in a more uniform manner in the crack front process region, giving rise to decohesion of packet and block martensite boundaries (PRHIC) only after significant previous plastic deformation (high fracture toughness for the onset of crack growth).

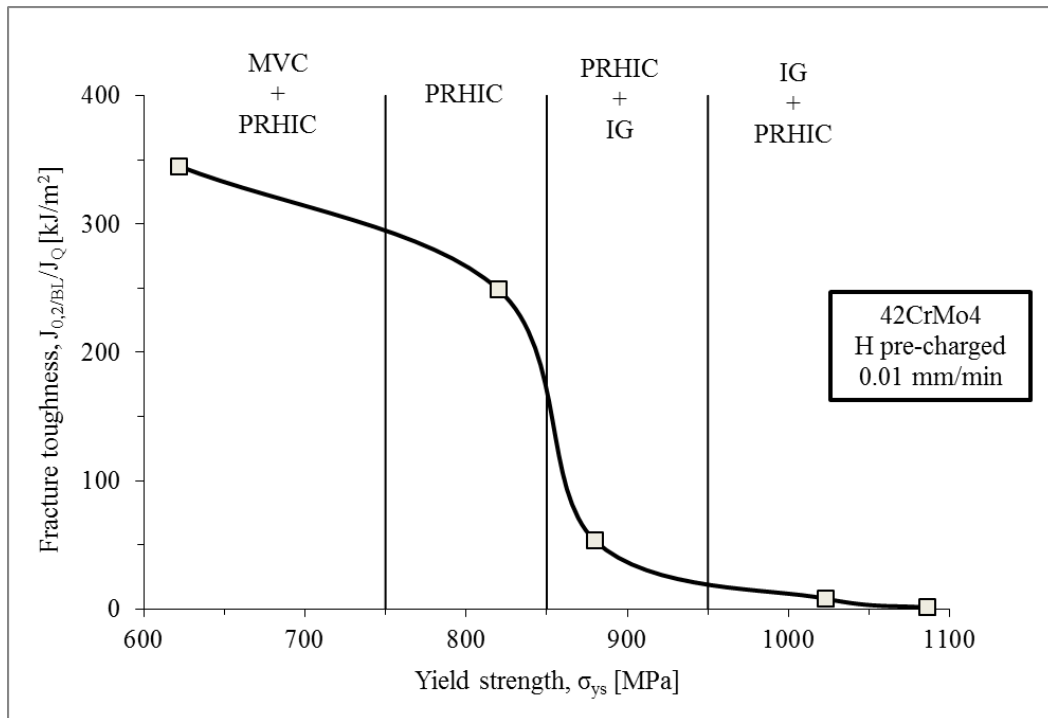


Figure 7. Fracture toughness for the onset of crack growth with internal hydrogen versus steel yield strength (42CrMo4) and predominant failure micromechanisms.

The extreme brittleness of the H-charged 42CrMo4 steel grades tempered at the lowest temperatures (500, 550°C and even at 600°C) excludes the use of these steel grades when toughness is a design requirement.

The J resistance curves of the remaining quenched and tempered steel grades used in this research study under internal hydrogen tested at a low displacement rate of 0.01 mm/min are now compared in Fig. 8. All these grades show high fracture toughness for crack propagation, PRHIC and MVC being the most important failure micromechanisms (with only small areas of IG fracture in 2.25Cr1Mo\_600). The differences in fracture toughness results and fracture micromechanisms between 42CrMo4 and 2.25Cr1Mo steels are not significant. 42CrMo4 has higher carbon content and 2.25Cr1Mo higher chromium and molybdenum contents. The main differences between the two steels after quenching and high temperature tempering correspond to their carbide nature and distribution: a higher volume fraction of iron carbides for 42CrMo4 and chromium and molybdenum carbides in 2.25Cr1Mo [14, 32].

The high fracture toughness measured in 2.25Cr1MoV steel with internal hydrogen is worth noting, being the only grade in which the presence of hydrogen did not modify the failure micromechanism (fully ductile, MVC, in all the fracture tests, as shown in Table 7). However, this steel retained much higher hydrogen contents after H-charging than the others (see Table 4). Nevertheless, in this case this hydrogen barely affects the fracture process, as it is strongly trapped by very fine sub-micrometric uniformly distributed vanadium carbides [24, 25].

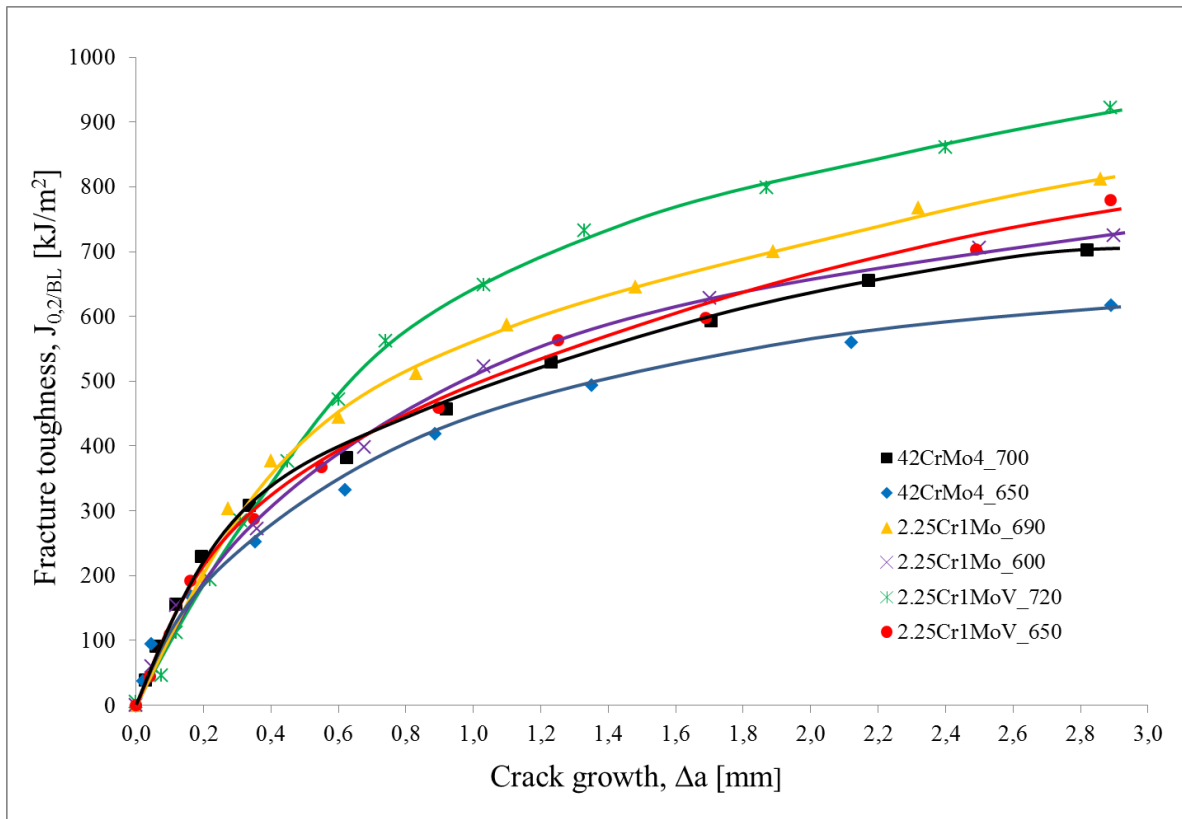


Figure 8. Fracture toughness-crack growth ( $J$ - $\Delta a$ ) curves corresponding to hydrogen pre-charged specimens tested at the lowest displacement rate (0.01mm/min).

The  $J$  fracture toughness of these grades for the onset of crack growth,  $J_{0.2/BL}$ , under internal hydrogen and a displacement rate of 0.01 mm/min is plotted in Fig. 9 versus their respective steel yield strengths. As expected, fracture toughness decreases with increasing yield strength, and a good regression with a quite high determination coefficient ( $R^2=0.9$ ) being obtained, even though three different steels were employed.

Finally, it is worth noting that high fracture toughness with internal hydrogen using low displacement rates (with high hydrogen concentrations in their fracture process zones) was obtained in these quenched and tempered steel grades with yield strengths as high as 800 MPa. The use of these high strength steel grades in damage tolerant designs would allow decreasing component thickness and hence the cost of the steel used to manufacture hydrogen infrastructures such as hydrogen tanks, pipes and valves directly exposed to high-pressure hydrogen gas environments. Nonetheless, fatigue crack initiation times and fatigue crack propagation rates in the presence of hydrogen are also other important characteristics to be determined in order to properly design such infrastructures.

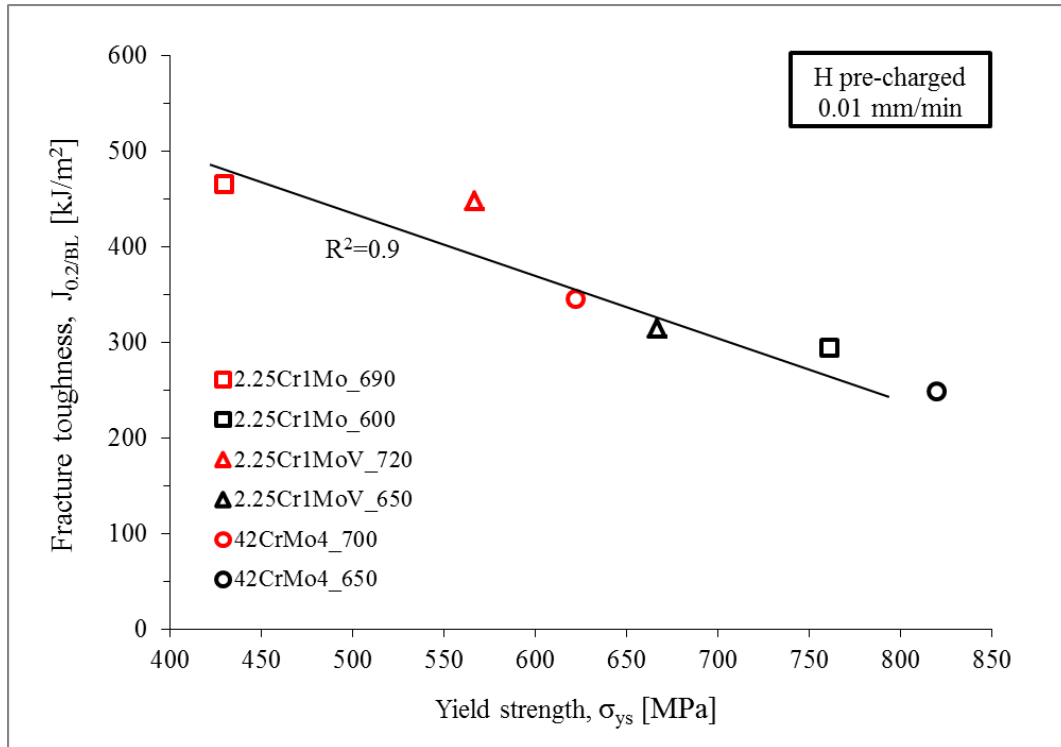


Figure 9. Fracture toughness,  $J_{0.2/BL}$ , with internal hydrogen (0.01 mm/min) versus steel yield strength.

## 5. CONCLUSIONS

The initial hydrogen content measured in CrMo and CrMoV steels pre-charged under high temperature hydrogen pressure increased with decreasing steel tempering temperature due to the fact that hydrogen microstructural trapping is greater in distorted, high energy martensitic microstructures. Moreover, the strongly trapped hydrogen content is even more dependent on the steel microstructure, increasing with decreasing tempering temperature and also as the result of the existence of vanadium carbides in CrMoV grades, which are recognized as being very strong hydrogen traps.

Fracture toughness measured with internal hydrogen strongly decreases with tempering temperature (higher yield strength as well as higher hydrogen retention), also being highly dependent on the applied displacement rate, as the accumulation of hydrogen atoms in the process zone located ahead of the crack tip of the CT fracture specimen increases due to the availability of longer diffusion times, thereby promoting the embrittlement phenomenon. This trend is consistent with the change appreciated in the fracture micromechanisms: MVC was the only failure micromechanism in uncharged specimens, changing to PRHC and even IG (for the most embrittled grades) in tests performed with internal hydrogen, except in the CrMoV steel grade, in which the presence of hydrogen did not modify the failure micromechanism observed in tests performed in air.

High fracture toughness with internal hydrogen under low displacement rates (with high hydrogen accumulation within the process zone) were obtained in quenched and tempered CrMo and CrMoV steel grades even with yield strengths as high as 800 MPa. These grades could constitute good options for the manufacture of components to manage high-pressure hydrogen gas.

## ACKNOWLEDGEMENTS

The authors would like to thank the Spanish Ministry of Economy and Competitiveness for the support received to carry out research project MAT2014-58738-C3 (SAFEHIDROSTEEL) and to the Principado de Asturias government for the financing support given to the IDI/2018/000134 project.

## REFERENCES

- [1] R. Von Helmolt, U. Ebele. Fuel cell vehicles: Status 2007. *Journal of Power Sources* 2007; 165: 833-843.
- [2] R.P. Gangloff. Hydrogen assisted cracking in high strength alloys, in *Comprehensive Structural Integrity*. Elsevier Science 2013; 6.
- [3] J. Yamabe, H. Matsunaga, Y. Furuya, S. Hamada, H. Itoga, M. Yoshikawa, E. Takeuchi, S. Matsuoka. Qualification of chromium-molybdenum steel based on the safety factor multiplier method in CHMC1-2014. *Int J Hydrogen Energy* 2015; 40: 717-728.
- [4] J. Yamabe, T. Awane, S. Matsuoka. Investigation of hydrogen transport behaviour of various low-alloy steels with high-pressure hydrogen gas. *Int J Hydrogen Energy* 2015; 40(34): 11075-11086.
- [5] L. Briottet, R. Batische, G. de Dinechin, P. Langlois, and L. Thiers. Recommendations on X80 steel for the design of hydrogen gas transmission pipelines. *Int J Hydrogen Energy* 2012; 37(11): 9423–9430.
- [6] J. H. Chuang, L.W. Tsay, c. Chen. Crack growth behaviour of heat-treated 4140 steel in air and gaseous hydrogen. *Int. J. Fatigue* 1998; 20(7): 531-536.
- [7] M. Wang, E. Akiyama, and K. Tsuzaki. Effect of hydrogen on the fracture behavior of high strength steel during slow strain rate test. *Corros Sci* 2007; 49(11): 4081–4097.
- [8] E. Akiyama, M. Wang, S. Li, Z. Zhang, Y. Kimura, N. Uno, K. Tsuzaki. Studies of evaluation of hydrogen embrittlement property of high-strength steels with consideration of the effect of atmospheric corrosion. *Metallurgical and Materials Transactions* 2013; 44A: 1290-1300.
- [9] A. Zafra, L.B. Peral, J. Belzunce, C. Rodríguez. Effect of hydrogen on the tensile properties of 42CrMo4 steel quenched and tempered at different temperatures. *Int. J. Hydrogen Energy* 2018; 43: 9068-9082.
- [10] R.P. Gangloff, B.P. Somerday. *Gaseous hydrogen embrittlement of materials in energy technologies*. Woodhead Publishing, 2012.
- [11] C. San Marchi, B.P. Somerday. Technical reference on hydrogen compatibility of materials, Sandia Report SAND2008-1163. Sandia National Laboratories, 2008.
- [12] H. Barthelemy. Effects of pressure and purity on the hydrogen embrittlement of steels. *Int J Hydrogen Energy* 2011; 36: 2750-2758.
- [13] Y. Ogawa, H. Matsunaga, J. Yamabe, M. Yoshikawa, S. Matsuoka. Unified evaluation of hydrogen-induced crack growth in fatigue tests and fracture toughness tests of a carbon steel. *Int J of Fatigue* 2017; 103: 223-233.
- [14] S. Pillot, L. Coudreuse. *Hydrogen-induced disbonding and embrittlement of steels used in petrochemical refining*. Woodhead Publishing Limited, 2012.
- [15] J. H. Liu, L. Wang, Y. Liu, X. Song, J. Luo, D. Yuan. Effects of hydrogen on fracture toughness and fracture behaviour of SA508-III steel. *Mater. Res. Innovations* 2014; 18(4): 255-259.
- [16] C. Colombo, G. Fumagalli, F. Bolzoni, G. Gobbi, L. Vergani. Fatigue behaviour of hydrogen pre-charged low alloy Cr-Mo steel. *Int J of Fatigue* 2016; 83: 2-9.
- [17] A. W. Loginow, E.E. Phelps. Steels for seamless hydrogen pressure vessels. *Corrosion* 1975; 31: 404-412.
- [18] Y. Li, B. Gong, A. Li, C. Deng, D. Wang. Specimen thickness effect on the property of hydrogen embrittlement in single edge notch tension testing of high strength pipeline steel. *Int J Hydrogen Energy* 2018; 43: 15575-15585.
- [19] R. L.S. Thomas, J.R. Scully, R. Gangloff. Internal hydrogen embrittlement of ultrahigh-strength AERMET 100 steel. *Metallurgical and Materials Transactions A* 2003; 34: 327-344.
- [20] I.M. Robertson, P. Sofronis, A. Nagao, N.L. Martin, S. Wang, D.W. Gros, K.E. Nygren. Hydrogen embrittlement understood. *Metallurgical and Materials Transactions* 2015; 46B: 1085-1103.

- [21] T. Mitchler, C. San Marchi, J. Naumann S. Weber, M. Martin. Hydrogen environment embrittlement of stable austenitic steels. *Int J Hydrogen Energy* 2012; 37: 16231-16246.
- [22] ASTM E1820. Standard test method for measurement of fracture toughness. *Annual Book of ASTM Standards* 2015; 03.01.
- [23] George Krauss. *Steels: Processing, Structure and Performance*. ASM International, 2005.
- [24] J. Lee, T. Lee, Y.J. Kwon, D.J. Mun, J.Y. Yoo, C. S. Lee. Effects of vanadium carbides on hydrogen embrittlement of tempered martensitic steel. *Met. Mater. Int* 2016; 22( 3): 364-372.
- [25] X.Y. Cheng, H. Li, X.B. Cheng. Carbides and possible hydrogen irreversible trapping sites in ultrahigh strength round steel. *Micron* 2017; 103: 22-28.
- [26] R.M. McMeeking, D.M. Parks. On criteria for J-dominance of crack-tip fields in large-scale yielding. *ASTM STP 668*, American Society for Testing and Materials, Philadelphia, 1979, 175-194.
- [27] P. Sofronis, R.M. McMeeking. Numerical analysis of hydrogen transport near a blunting crack tip, *J. Mechanic Phys. Solids* 1989; 37: 317-350.
- [28] K. A. Nibur, B. P. Somerday, C. S. A. N. Marchi, J. W. Foulk, M. Dadfarnia, and P. Sofronis. The Relationship Between Crack-Tip Strain and Subcritical Cracking Thresholds for Steels in High-Pressure Hydrogen Gas. *Metall. Mater. Trans. A* 2013; 44A: 248–269.
- [29] Y. Takeda and C. J. McMahan Jr. Strain controlled vs. stress controlled hydrogen induced fracture in a quenched and tempered steel. *Metall. Mater. Trans. A* 1981;12A: 1255–1266.
- [30] A. Nagao, M.L. Martin, M. Dadfarnia, P. Sofronis, I.M. Robertson. The effect of nanosized (Ti,Mo)C precipitates on hydrogen embrittlement of tempered lath martensitic steels. *Acta Materialia* 2014; 244-254.
- [31] Y. Murakami and S. Matsuoka. Effect of hydrogen on fatigue crack growth of metals. *Eng. Fract. Mech* 2010; 77(11): 1926–1940.
- [32] N. Parvathvarthini, S. Saroja, R.K. Dayal, H.S. Khatak. Studies on hydrogen permeability of 2.12%Cr-1%Mo ferritic steel: correlation with microstructure. *Journal of Nuclear Materials* 2001; 288: 187-196.